Molecular Cell, Volume *66*

Supplemental Information

Ribonucleotide Reductase Requires Subunit Switching in Hypoxia to Maintain DNA Replication

Iosifina P. Foskolou, Christian Jorgensen, Katarzyna B. Leszczynska, Monica M. Olcina, Hanna Tarhonskaya, Bauke Haisma, Vincenzo D'Angiolella, William K. Myers, Carmen Domene, Emily Flashman, and Ester M. Hammond

Figure S1

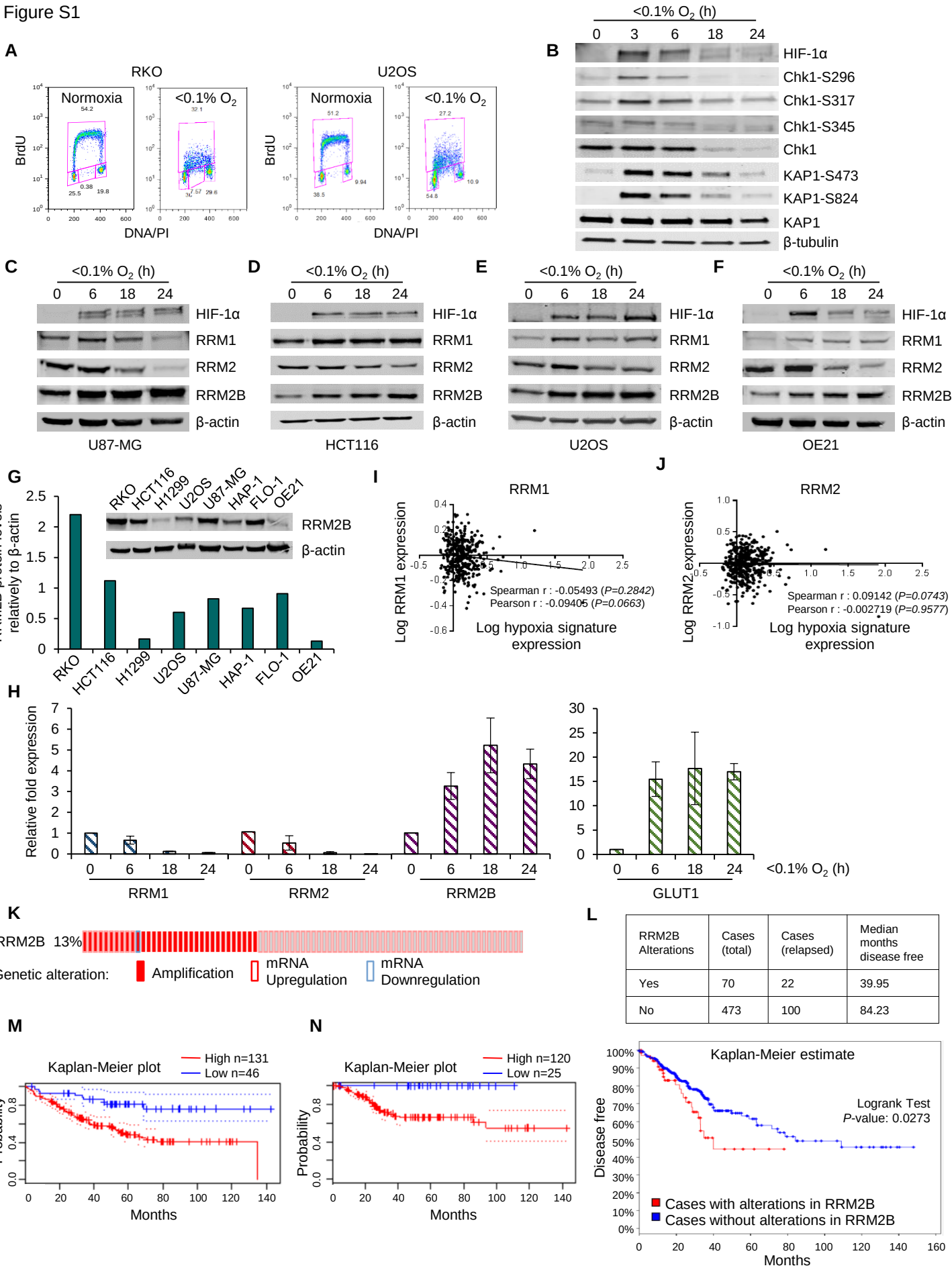

RRM2B Alterations	Cases (total)	Cases (relapsed)	Median months disease free
Yes	70	22	39.95
No	473	100	84.23

Figure S2

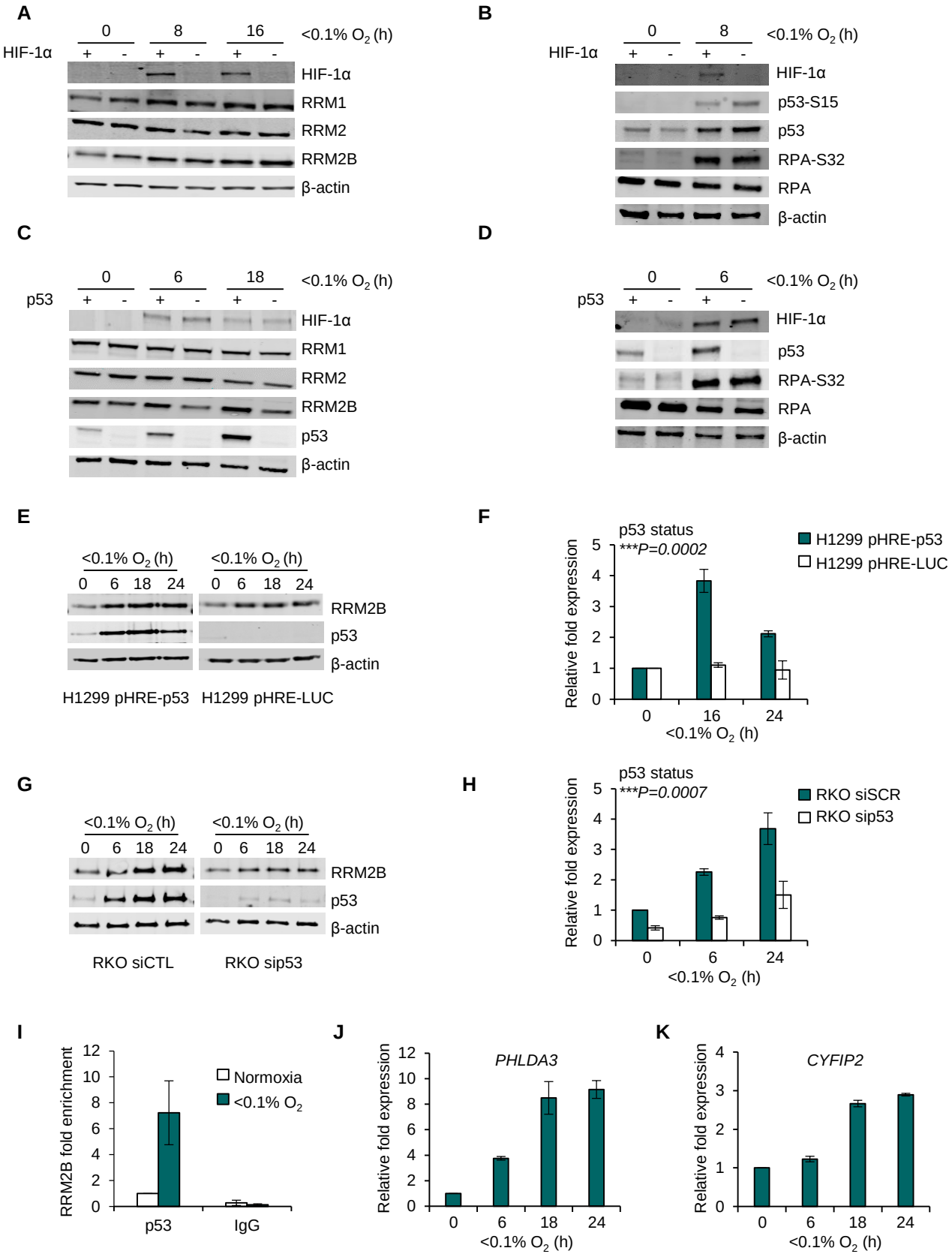
A
0
8
16
<0.1% O2 (h)
HIF-1α
+ - + - + -
HIF-1α
RRM1
RRM2
RRM2B
β-actin
B
0
8
<0.1% O2 (h)
HIF-1α
+ - + -
HIF-1α
p53-S15
p53
RPA-S32
RPA
β-actin
C
0
6
18
<0.1% O2 (h)
p53
+ - + - + -
HIF-1α
RRM1
RRM2
RRM2B
p53
β-actin
D
0
6
<0.1% O2 (h)
p53
+ - + -
HIF-1α
p53
RPA-S32
RPA
β-actin
E
<0.1% O2 (h)
<0.1% O2 (h)
0 6 18 24
0 6 18 24
RRM2B
p53
β-actin
H1299 pHRE-p53
H1299 pHRE-LUC
F
p53 status
***P=0.0002
H1299 pHRE-p53
H1299 pHRE-LUC
Relative fold expression
0 1 2 3 4 5
0 16 24
<0.1% O2 (h)
G
<0.1% O2 (h)
<0.1% O2 (h)
0 6 18 24
0 6 18 24
RRM2B
p53
β-actin
RKO siCTL
RKO sip53
H
p53 status
***P=0.0007
RKO siSCR
RKO sip53
Relative fold expression
0 1 2 3 4 5
0 6 24
<0.1% O2 (h)
I
RRM2B fold enrichment
0 2 4 6 8 10 12
Normoxia
<0.1% O2
p53
IgG
J
PHLDA3
Relative fold expression
0 2 4 6 8 10 12
0 6 18 24
<0.1% O2 (h)
K
CYFIP2
Relative fold expression
0 1 2 3 4
0 6 18 24
<0.1% O2 (h)

Figure S3

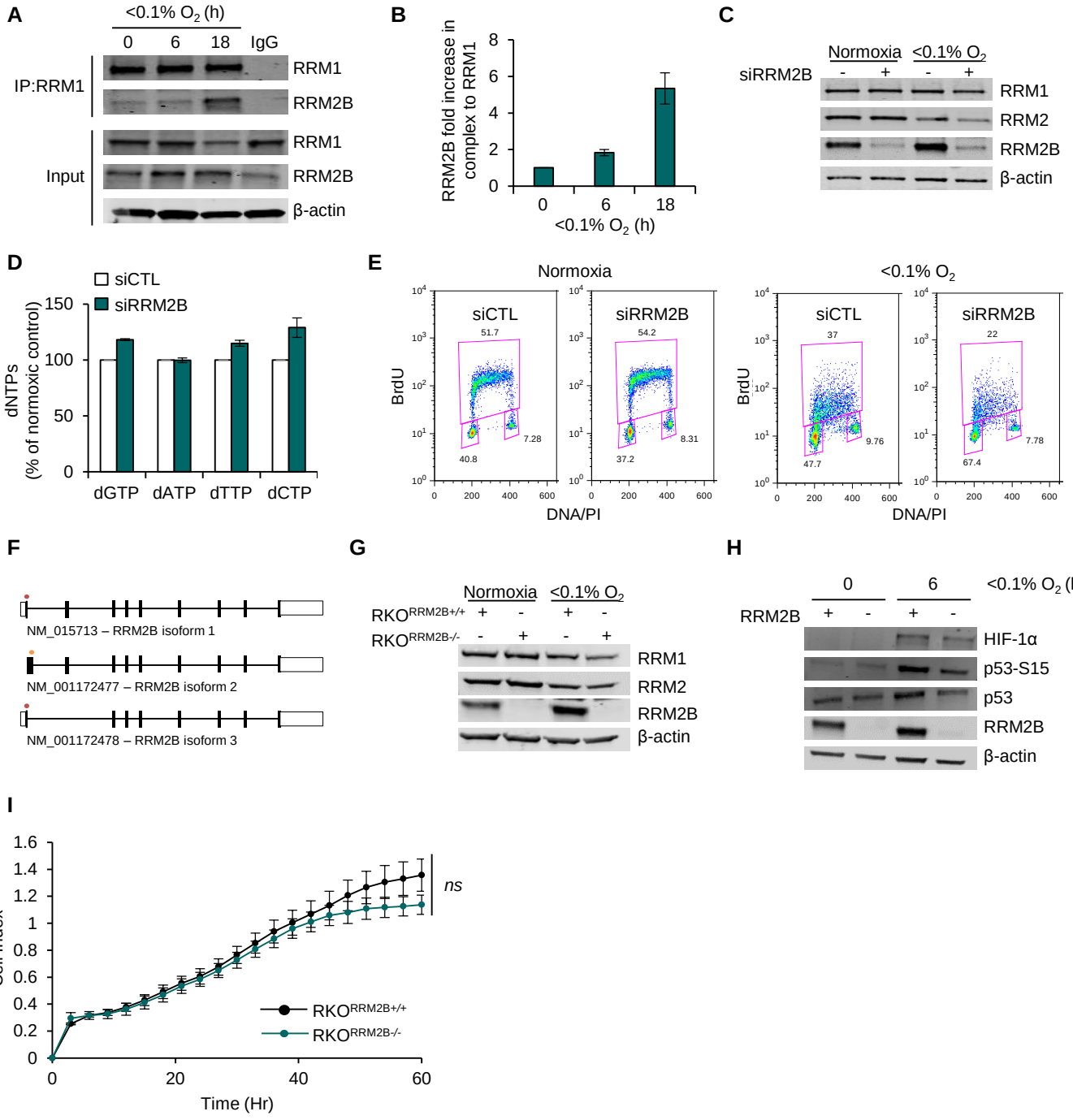
A
<0.1% O2 (h)
0
6
18
IgG
IP:RRM1
RRM1
RRM2B
Input
RRM1
RRM2B
β-actin
B
RRM2B fold increase in complex to RRM1
8
6
4
2
0
0
6
18
<0.1% O2 (h)
C
Normoxia
<0.1% O2
siRRM2B
-
+
-
+
RRM1
RRM2
RRM2B
β-actin
D
siCTL
siRRM2B
dNTPs (% of normoxic control)
150
100
50
0
dGTP
dATP
dTTP
dCTP
E
Normoxia
<0.1% O2
siCTL
siRRM2B
siCTL
siRRM2B
51.7
7.28
40.8
54.2
8.31
37.2
37
9.76
47.7
22
7.78
67.4
BrdU
DNA/PI
F
NM_015713 – RRM2B isoform 1
NM_001172477 – RRM2B isoform 2
NM_001172478 – RRM2B isoform 3
G
Normoxia
<0.1% O2
RKORRM2B+/+
RKORRM2B-/-
RRM1
RRM2
RRM2B
β-actin
H
0
6
<0.1% O2 (h)
RRM2B
HIF-1α
p53-S15
p53
RRM2B
β-actin
I
Cell Index
1.6
1.4
1.2
1
0.8
0.6
0.4
0.2
0
0
20
40
60
Time (Hr)
ns
RKORRM2B+/+
RKORRM2B-/-

Figure S4

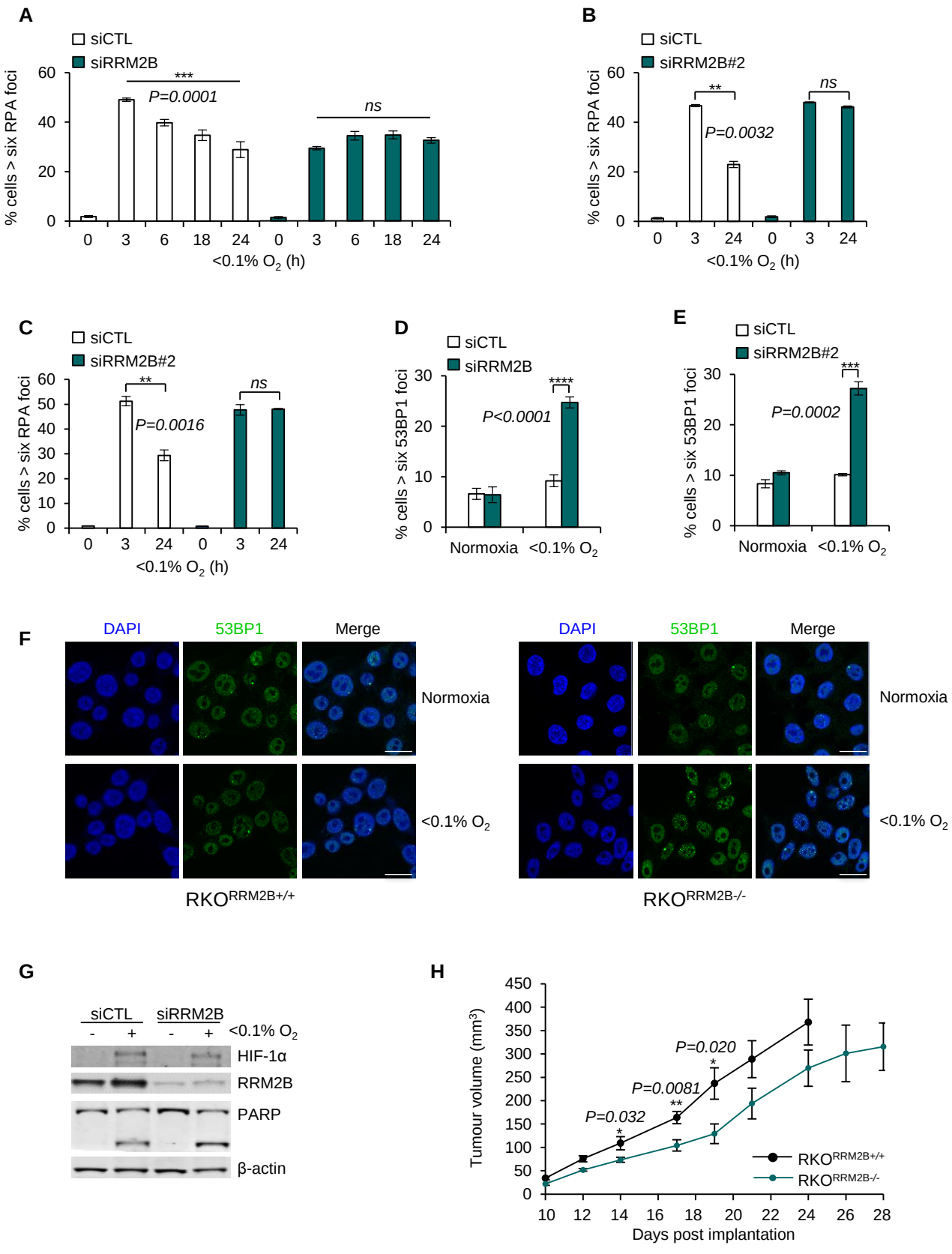
A
siCTL
siRRM2B
% cells > six RPA foci
***
P=0.0001
ns
<0.1% O2 (h)
B
siCTL
siRRM2B#2
% cells > six RPA foci
**
P=0.0032
ns
<0.1% O2 (h)
C
siCTL
siRRM2B#2
% cells > six RPA foci
**
P=0.0016
ns
<0.1% O2 (h)
D
siCTL
siRRM2B
% cells > six 53BP1 foci
****
P<0.0001
Normoxia
<0.1% O2
E
siCTL
siRRM2B#2
% cells > six 53BP1 foci
***
P=0.0002
Normoxia
<0.1% O2
F
DAPI
53BP1
Merge
Normoxia
<0.1% O2
RKORRM2B+/+
RKORRM2B-/-
G
siCTL
siRRM2B
<0.1% O2
HIF-1α
RRM2B
PARP
β-actin
H
Tumour volume (mm3)
P=0.032
P=0.0081
P=0.020
RKORRM2B+/+
RKORRM2B-/-
Days post implantation

Figure S5

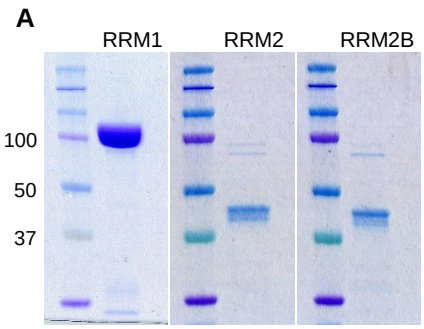

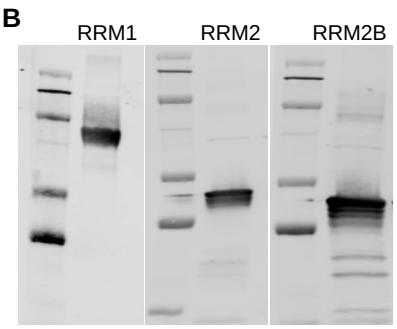

C

Protein Sample	nM Fe / µM of protein
RRM2B	464.8 ± 38.8
Apo-RRM2B	57.5 ± 8.8
RRM2	447.5 ± 21.8
Apo-RRM2	56.7 ± 5.7

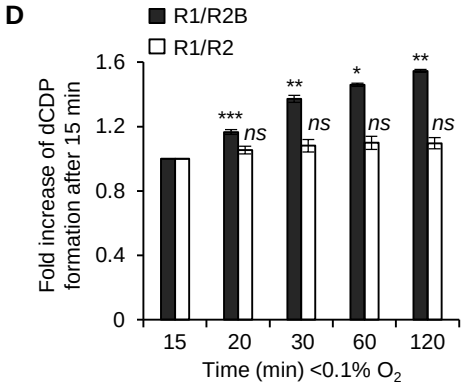

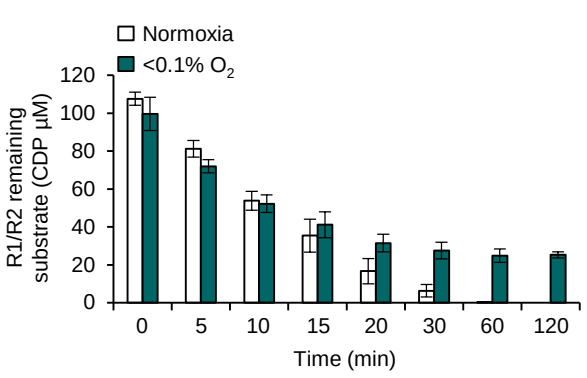

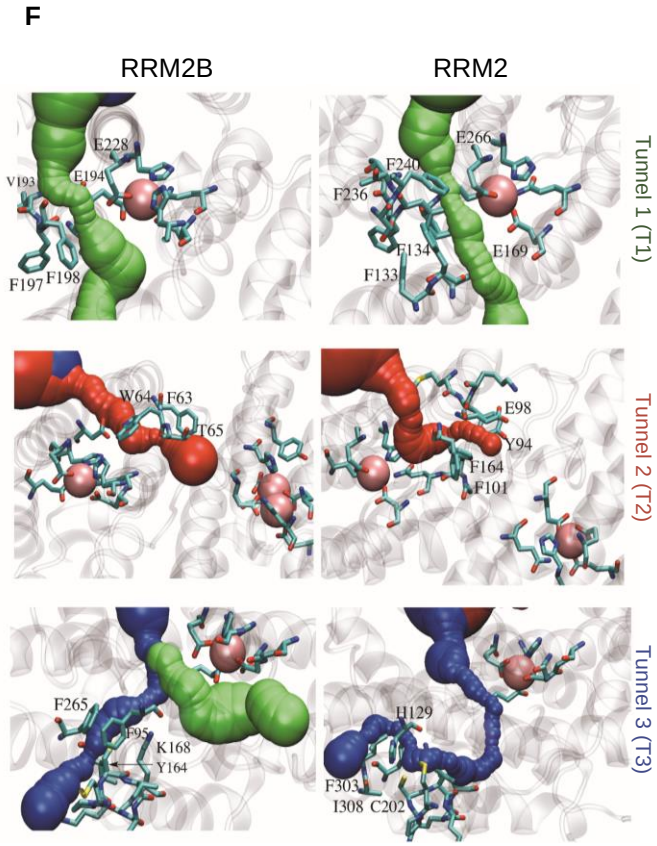

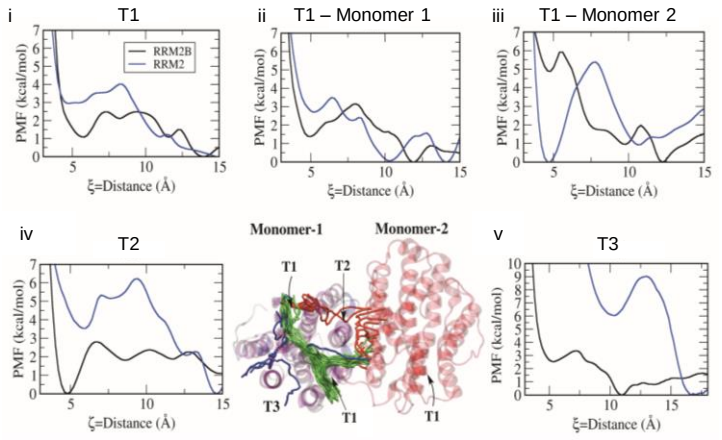

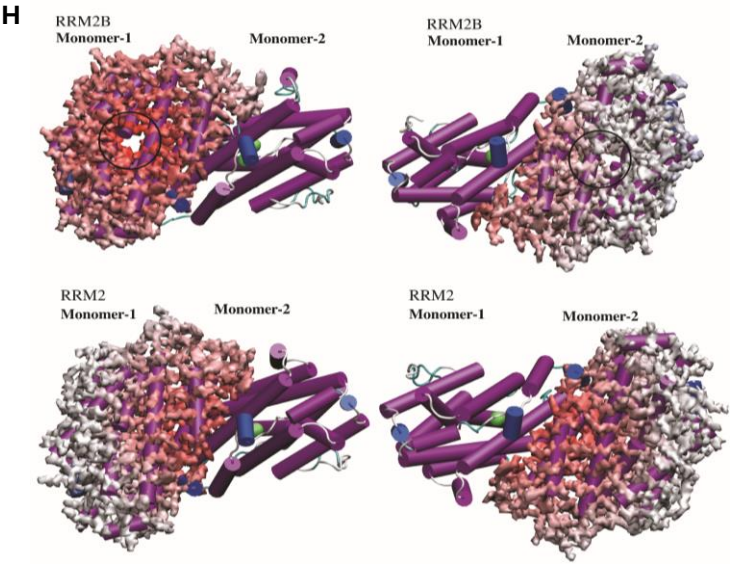

Figure S6

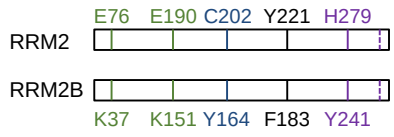

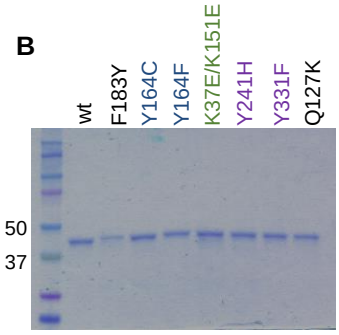

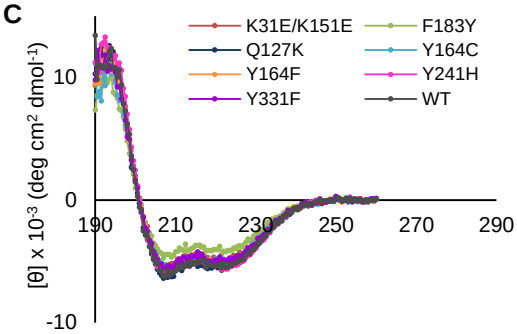

D

Protein Sample	nM Fe / µM of protein
Y164F	310.4 ± 33.3
F183Y	433.8 ± 17.8
Y241H	489.0 ± 20.3
Y164C	269.9 ± 23.6
K37E/K151E	367.9 ± 47.9
Y331F	397.2 ± 37.3
Q127K	134.3 ± 21.2

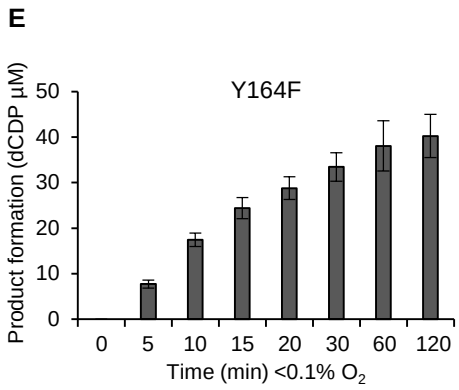

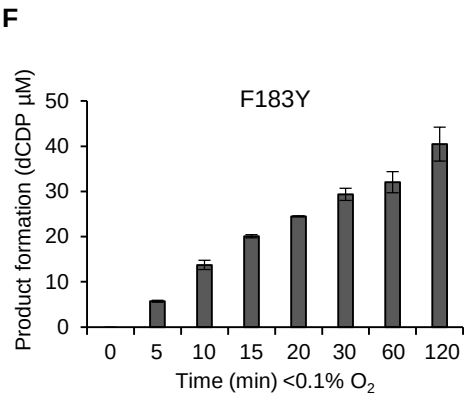

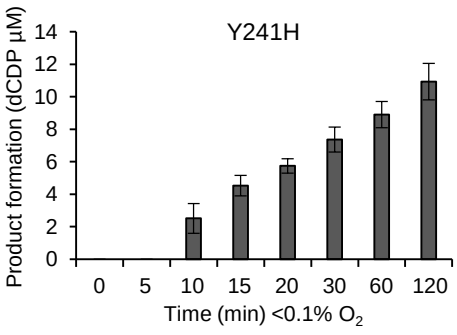

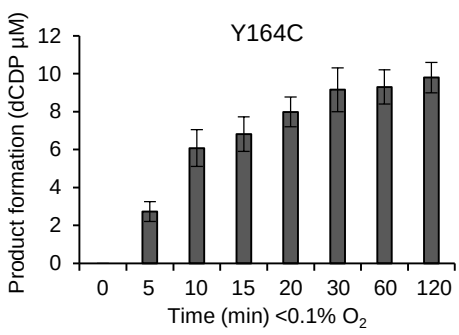

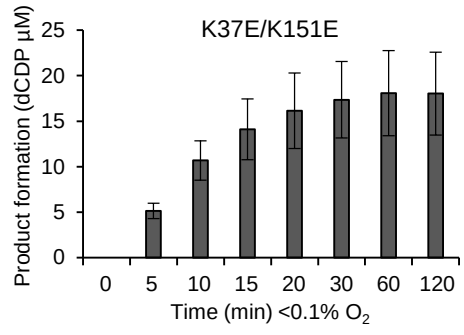

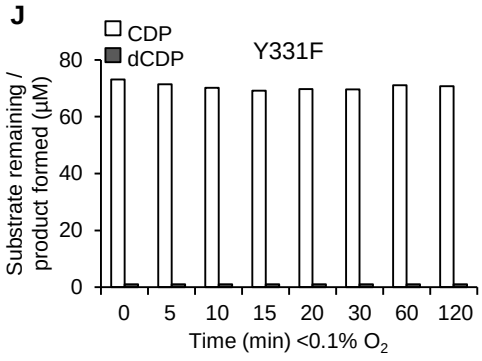

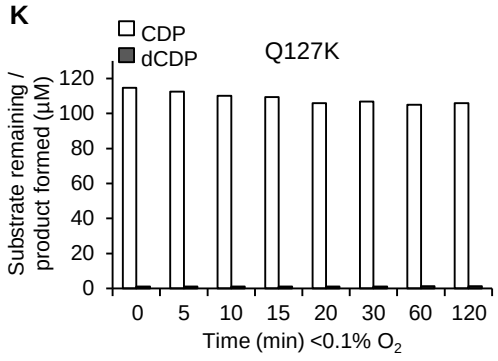

Figure S7

A

RRM2B EPR Sample	Spins / β subunit ($x10^{-3}$)	Hypoxia / Normoxia (%)
Y241H Normoxia	6.85 ± 0.05	72.5 ± 0.5
Y241H <0.1% O_2	5 ± 0	
F183Y Normoxia	11.7 ± 1.1	79.5 ± 4.5
F183Y <0.1% O_2	9.25 ± 0.35	
Y164F Normoxia	35.5 ± 0.5	60 ± 4
Y164F <0.1% O_2	21.25 ± 1.25	
Q127K Normoxia	ND	ND
Q127K <0.1% O_2	ND	

B

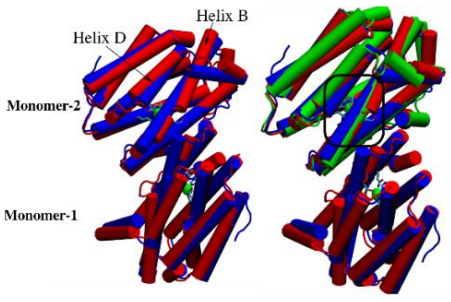

C

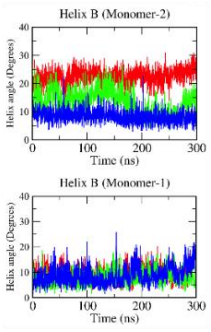

D

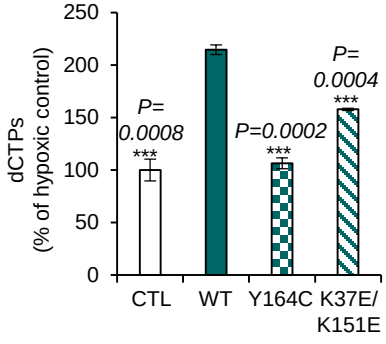

E

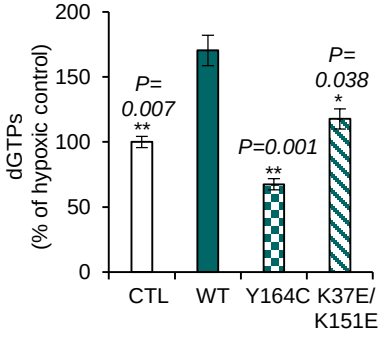

Figure S1. Related to Figure 1.

(A) Representative images of FACS analysis of RKO and U2OS cells exposed to normoxia or <0.1% O_2 (3 hr) indicating replication stress in hypoxic conditions. Cells were pulsed with BrdU (20 μM) 30 min before collection. **(B)** Immunoblots for common DDR targets in RKO cells exposed to <0.1% O_2 for the times indicated. **(C-F**) Immunoblots of RNR subunits in different cancer cell lines exposed to <0.1% O_2 for the times indicated: (C) U87-MG (human glioblastoma); (D) HCT116 (colorectal carcinoma); (E) U2OS (human osteosarcoma) and (F) OE21 (human esophageal). **(G)** RRM2B levels relatively to β-actin in a panel of different cell lines in normoxia. RKO cells showed the highest expression of RRM2B protein. **(H)** mRNA levels of RNR subunits in U87-MG cells in <0.1% O_2 normalized to 18S. For all panels n=3 (biological replicates); for panel (H) data show means ± s.e.m. **(I)** Expression of RRM1 (Log10 conversion) in the colorectal adenocarcinoma TCGA datasets is shown against hypoxia-inducible signature (Log10 conversion). **(J)** Expression of RRM2 (Log10 conversion) in the colorectal adenocarcinoma TCGA datasets is shown against hypoxia-inducible signature (Log10 conversion). **(K)** The Cancer Genome Atlas (TCGA) colorectal adenocarcinoma dataset was analyzed for genetic alterations (including mutations, putative copy-number alterations and mRNA expression data (RNA Seq V2 RSEM)) in *RRM2B* gene using cBioPortal. The scheme shows only the 13% cases (83 out of 629), where the genetic alterations in *RRM2B* was found. No mutations were reported. **(L)** Kaplan-Meier curve showing disease free survival in cancer cases with or without alterations in R*RM2B* from K. **(M-N)** The expression of RRM2B and the associated survival probability in colorectal cancers using PrognoScan. The colorectal cancer patient dataset GSE17536 was analyzed using PrognoScan tool and overall survival (M), as well as disease-free survival (N) associated with high or low expression of RRM2B (probe 223342_at) are shown in Kaplan-Meier plots.

Figure S2. Related to Figure 2.

(A) Immunoblots of the RNR subunits in RKO$^{HIF\text{-}1\alpha+/+}$ and RKO$^{HIF\text{-}1\alpha-/-}$ cells exposed to <0.1% O_2 for the times indicated. RRM2B protein is induced in hypoxia irrespective of HIF-1α status. **(B)** Immunoblots of common replication stress markers in RKO$^{HIF\text{-}1\alpha+/+}$ and RKO$^{HIF\text{-}1\alpha-/-}$ cells exposed to <0.1% O_2 (8 hr). **(C)** Immunoblots of the RNR subunits in HCT116$^{p53+/+}$ and HCT116$^{p53-/-}$ cells exposed to <0.1% O_2 for the times indicated. RRM2B protein is decreased in the absence of p53. **(D)** Immunoblots of the replication stress marker RPA32 in HCT116$^{p53+/+}$ and HCT116$^{p53-/-}$ cells exposed to <0.1% O_2 (6 hr). **(E-F)** Immunoblots (E) and *RRM2B* mRNA levels (F) of H1299 cells treated with either pHRE-p53 or pHRE-LUC and exposed to <0.1% O_2 for the times indicated. **(G-H)** Immunoblots (G) and *RRM2B* mRNA levels (H) of RKO cells treated with either sip53 or siCTL and exposed to <0.1% O_2 for the times indicated. **(I)** qPCR for p53 ChIP in HCT116 cells exposed to either normoxia or <0.1% O_2 (6 hr). **(J-K)** mRNA levels of hypoxia inducible p53 targets *PHLDA3* (J) and *CYFIP2* (K) in RKO cells exposed to <0.1% O_2 normalized to 18S. For all panels n=3 (biological replicates); panels (F, H, J and K) data show mean ± s.e.m. (I) shows representative mean of technical triplicates ± RQmax/RQmin. p53 status was examined by two-way ANOVA analysis; (ns) indicates non significant change.

Figure S3. Related to Figure 3.

(A) Immunoprecipitation of RRM1 for the times indicated, followed by immunoblotting for RRM2B in normoxia and <0.1% O_2. **(B)** Quantification of (A) from n=3 biological replicates. **(C)** Immunoblots of RNR subunits in RKO cells treated with either siCTL or siRRM2B and exposed to normoxia or <0.1% O_2 (18 hr). Effective depletion of RRM2B protein with the specific siRNA is observed in both conditions. **(D)** dNTP incorporation assay in RKO cells treated with either siCTL or siRRM2B in normoxia. **(E)** Representative images of FACS

analysis of U2OS cells treated with either siCTL or siRRM2B and exposed to normoxia or <0.1% O_2 (3 hr). **(F)** Representative figure of the three isoforms of *RRM2B* gene. Black rectangles represent exons. The colored ovals represent the positions targeted by the guided RNAs in order the $RKO^{RRM2B-/-}$ cell line to be constructed (CRISPR-Cas9 system). **(G)** Immunoblots of RNR subunits in $RKO^{RRM2B+/+}$ and $RKO^{RRM2B-/-}$ cell lines exposed to normoxia or <0.1% O_2 (18 hr). **(H)** Immunoblots of p53 status in $RKO^{RRM2B+/+}$ and $RKO^{RRM2B-/-}$ cell lines exposed to normoxia or <0.1% O_2 (6 hr). **(I)** Cell proliferation assay in normoxia using the xCELLigense system using $RKO^{RRM2B+/+}$ and $RKO^{RRM2B-/-}$ cells. For all panels n=3 (biological replicates); for panels (B, D, and I) data show mean ± s.e.m. and in panel (I) one-way ANOVA analysis was applied; (ns) indicates non significant change.

Figure S4. Related to Figure 3.

(A) Quantification of RPA32 foci in RKO cells treated with either siCTL or siRRM2B after exposure to <0.1% O_2 for the times indicated. **(B-C)** Quantification of RPA32 foci in RKO (B) or HCT116 (C) cells treated with either siCTL or siRRM2B#2 after exposure to <0.1% O_2 for the times indicated. **(D-E)** Quantification of 53BP1 foci in RKO cells treated with either siCTL or siRRM2B (D) or siRRM2B#2 (E) after exposure to normoxia or <0.1% O_2 (6 hr). **(F)** Representative images of 53BP1 foci in $RKO^{RRM2B+/+}$ and $RKO^{RRM2B-/-}$ cells exposed to normoxia or <0.1% O_2 (6 hr). Scale bar 20 µm. **(G)** Immunoblot for PARP cleavage in RKO cells treated with either siCTL or siRRM2B and exposed to normoxia or <0.1% O_2 (19 hr). **(H)** $RKO^{RRM2B+/+}$ and $RKO^{RRM2B-/-}$ xenografts were grown in mice. Tumor volumes were measured for 5 ($RKO^{RRM2B+/+}$) and 6 ($RKO^{RRM2B-/-}$) mice per each group and a mean ± s.e.m. is shown. For all panels n=3 (biological replicates) otherwise stated; for panels (A-E and H) data show mean ± s.e.m. and two-tailed Student's t-test was applied; in panel (A) one-way ANOVA analysis was applied; (ns) indicates non significant change.

Figure S5. Related to Figure 4.

(A-B) Recombinant RRM1, RRM2 and RRM2B proteins were overexpressed in *E.coli* cells and purified to ~90% purity as shown with Coomassie blue staining (A) and Immunoblotting (B). **(C)** Quantitation of iron bound in the RRM2B and RRM2 proteins as overexpressed in *E.coli* cells using ICP-MS. As negative control the apo-forms of the proteins were used. **(D)** Fold increase of dCDP formation in <0.1% O_2 for the indicated times normalized to 15 min for either R1/R2B or R1/R2 enzymes. Graphs show the amount of dCDP formed after 15 min in <0.1% O_2 and each time point was compared with the previous to determine statistically significant dCDP formation. **(E)** Substrate consumption (CDP) in normoxia and hypoxia for R1/R2. For panel (C) n=3 (technical replicates); for panels (D-E) n=3 (biological replicates); in all panels data show mean ± s.e.m.; in panel (D) two-tailed Student's t-test was applied; (ns) indicates non significant change. **(F)** Identification and analysis of the RRM2B and RRM2 oxygen tunnels. MD simulations revealed three principle oxygen cavity tunnels (T1-3) in Monomer-1 in both RRM2B and RRM2 proteins. T1: reveals connectivity between Monomer-1 active site and the outside protein surface, with an average length 29.0 ± 16 Å in RRM2B to 15.0 ± 15 Å in RRM2. T2: reveals connectivity between Monomer-1 and Monomer-2. T3: connects either the Tyr164 (RRM2B) or the Cys202 (RRM2) with the pocket of phenylalanines. **(G)** Potential of Mean Force for oxygen entry shows differential functioning of RRM2B to RRM2. Comparison between RRM2B (black) and RRM2 (blue) PMF for diffusion (i) T1 and (ii) T1 in Monomer-1, compared to (iii) T1 in Monomer-2; (iv) T2 and (v) T3. The Potential of Mean Force (PMF) for diffusion in the individual tunnels between RRM2B (black) and RRM2 (blue) reveal differences in the tunnels of RRM2B and RRM2. T1 is similar in RRM2B and RRM2, precluding selectivity differences and with oxygen entry characterized by low barriers of 2-3 kcal mol^{-1}, as reported for extended tunnels in [Ni-Fe] hydrogenases (Wang et al., 2011, Wang et al., 2013). T1 in Monomer-2, showed

barriers of 5-6 kcal mol^{-1}, which might explain the lower O_2 turnover of Monomer-2 compared to Monomer-1 in the unbiased MD simulations. T2 appears to show a pronounced difference between RRM2B and RRM2, with a 3 kcal mol^{-1} higher barrier for O_2 entry into RRM2 compared to RRM2B, as was rationalized in the crystal structure in which the T2 was proposed to be more open in RRM2B compared to RRM2 (Smith et al., 2009). T3 shows barrier height differences between RRM2B and RRM2 and suggest that RRM2B is a superior oxygen-sequestering agent. **(H)** RRM2B has an open phenylalanine channel. The switch of C202 in RRM2 to Y164 in RRM2B results in an open phenylalanine channel specifically in RRM2B.

Figure S6. Related to Figure 5.

(A) Representative figure of the key differences between RRM2 and RRM2B proteins. **(B)** Seven RRM2B variants were constructed with site-directed mutagenesis, overexpressed in *E.coli* cells and purified as shown with Coomassie blue staining to ~90% purity. **(C)** CD spectra of RRM2B WT and variant proteins ensuring that all proteins where properly folded; n=3 (technical replicates). **(D)** Quantitation of iron bound in the RRM2B variant proteins as overexpressed in E.coli cells using ICP-MS. **(E-I)** Product formation (dCDP) in <0.1% O_2 for (E) Y164F; (F) F183Y; (G) Y241H; (H) Y164C; (I) K37E/K151E. n=2 (biological replicates); data show mean ± s.e.m. **(J-K)** The substrate (CDP) over product formation for variants (J) Y331F and (K) Q127K showed zero turnover as expected. This is because in Y331F variant the pathway that transfers an electron to the catalytic site of RRM1 is disrupted (Xue et al., 2006), while in Q127K variant the stability of the tyrosyl radical cluster is disrupted (Zhou et al., 2010).

Figure S7. Related to Figure 5.

(A) Quantification of EPR spectra of the tyrosyl radical of mutant recombinant RRM2B proteins (Y241H, F183Y, Y164F and Q127K) in normoxia and <0.1% O_2. Data presented show electron spins per β subunit; n=2 (biological replicates); data show means ± s.e.m. **(B-C)** Comparison of RRM2B (red) with RRM2 (blue), revealing an open B-helix in RRM2B and a closed B-helix in RRM2. K37E/K151E (green) after 300 ns MD simulation has a closed B-helix. Plots (C) reveal Helix-B bending angle. **(D-E)** dCTP (D) and dGTP (E) in $RKO^{RRM2B-/-}$ cells transfected with either CTL, WT, Y164C or K37E/K151E and exposed to <0.1% O_2 (16 hr); n=3 (biological replicates); data show means ± s.e.m. and two-tailed Student's t-test was applied.

Table S1. Primer Table. Related to the STAR Methods.

Oligonucleotide Name	Sequence	Reference
Primers used for quantitative PCR (qPCR)		
18S Forward	TAGAGGGACAAGTGGCGTTC	This paper
18S Reverse	CGGACATCTAAGGGCATCAC	
GLUT-1 Forward	ATACTCATGACCATCGCGCTAG	This paper
GLUT-1 Reverse	AAAGAAGGCCACAAAGCCAAAG	
RRM1 Forward	ACCAACCGCCCACAACTTT	This paper
RRM1 Reverse	TGCCATTAGTCCCAGCAATGT	
RRM2 Forward	GTGGAGCGATTTAGCCAAGAA	(D'Angiolella et al., 2012)
RRM2 Reverse	CACAAGGCATCGTTTCAATGG	
RRM2B Forward	TGGTGGAGCGCTTTAGTCAG	This paper
RRM2B Reverse	CTATCCATCGCAAGGCCCAA	
INPP5D Forward	CGCCCACTAATCCTTGATGT	(Leszczynska et al., 2015)
INPP5D Reverse	GCTTGGACACCATGTTGATG	
CYFIP2 Forward	GGTCATGGAGGAACTGCTAA	(Leszczynska et al., 2015)
CYFIP2 Reverse	TCTTGGGCATCACCTCTATC	
Primers used for site-directed mutagenesis		
RRM2B_Y164F_For	ATTTAATGCAATTGAAACCATGCCCTT TGTTAAGAAAAAAGCAGATTG	This paper
RRM2B_Y164F_Rev	CAATCTGCTTTTTTCTTAACAAAGGGC ATGGTTTCAATTGCATTAAAT	
RRM2B_Y164C_For	ATTTAATGCAATTGAAACCATGCCCT GTGTTAAGAAAAAAGCAGATTG	This paper
RRM2B_Y164C_Rev	CAATCTGCTTTTTTCTTAACACAGGGC ATGGTTTCAATTGCATTAAAT	
RRM2B_K37E_For	GAAGAGCCACTCCTAAGAGAGAGTTC TCGCCG	This paper
RRM2B_K73E_Rev	CGGCGAGAACTCTCTCTTAGGAGTGG CTCTTC	
RRM2B_K151E_For	ACACTTACATCAGAGATCCCAAGGAA AGGGAATTTTTATTTAATGCA	This paper
RRM2B_K151E_Rev	TGCATTAAATAAAAATTCCCTTTCCTT GGGATCTCTGATGTAAGTGT	
RRM2B_F183Y_For	ATGGATAGCAGATAGAAAATCTACTT ATGGGGAAAGAGTGG	This paper
RRM2B_F183Y_Rev	CCACTCTTTCCCCATAAGTAGATTTTC TATCTGCTATCCAT	
RRM2B_Y241H_For	ACTTTGCTTGCCTGATGTTCCAACACT TAGTAAATAAGCCTTC	This paper
RRM2B_Y241H_Rev	GAAGGCTTATTTACTAAGTGTTGGAA CATCAGGCAAGCAAAGT	

RRM2B_Y331F_For RRM2B_Y331F_Rev	ATTTCTTTGAGAAACGAGTTTCAGAG TTTCAGCGTTTTGCAG CTGCAAAACGCTGAAACTCTGAAACT CGTTTCTCAAAGAAAT	This paper
RRM2B_Q127K_For RRM2B_Q127K_Rev	GCTCGCTGTTTCTATGGCTTTAAAATT CTCATCGAGAATGTTC GAACATTCTCGATGAGAATTTTAAAG CCATAGAAACAGCGAGC	This paper
Primers used for dNTP incorporation assay		
dTTP-Forward	TTATTATTATTATTATTATTAGGCGGT GGAGGCGG	(Sherman and Fyfe, 1989)
dCTP-Forward	TTTGTTTGTTTGTTTGTTTGGGCGGTG GAGGCGG	
dGTP-Forward	TTTCTTTCTTTCTTTCTTTCGGCGGTGG AGGCGG	
dATP-Forward	AAATAAATAAATAAATAAATGGCGGT GGAGGCGG	
dNTP-Reverse	CCGCCTCCACCGCC	

Table S2. Recombinant DNA Table. Related to the STAR Methods.

Plasmid Name	Backbone	Reference
pET28b-6xHis RRM1	pET-28a DNA (Novagen #69865-3)	(Wang et al., 2007)
pET28a-6xHis RRM2	pET-28a DNA (Novagen #69864-3)	(Shao et al., 2004)
pET28a-6xHis RRM2B	pET-28a DNA (Novagen #69864-3)	(Shao et al., 2004)
HA-RRM2B	pcDNA3.1 (Invitrogen; V79520)	(D'Angiolella et al., 2012)
pET28a-6xHis RRM2B^{Y164F}	pET-28a DNA (Novagen #69864-3)	This paper
pET28a-6xHis RRM2B^{Y164C}	pET-28a DNA (Novagen #69864-3)	This paper
pET28a-6xHis RRM2B$^{K37E/K151E}$	pET-28a DNA (Novagen #69864-3)	This paper
pET28a-6xHis RRM2B^{F183Y}	pET-28a DNA (Novagen #69864-3)	This paper
pET28a-6xHis RRM2B^{Y241H}	pET-28a DNA (Novagen #69864-3)	This paper
pET28a-6xHis RRM2B^{Y331F}	pET-28a DNA (Novagen #69864-3)	This paper
pET28a-6xHis RRM2B^{Q127K}	pET-28a DNA (Novagen #69864-3)	This paper
pRRM2B^{WT}	pcDNA3.1 (Invitrogen; V79520)	This paper
pRRM2B^{Y164C}	pcDNA3.1 (Invitrogen; V79520)	This paper
pRRM2B$^{K37E/K151E}$	pcDNA3.1 (Invitrogen; V79520)	This paper
pRRM2B^{Q127K}	pcDNA3.1 (Invitrogen; V79520)	This paper
pHRE-p53	pGL3-basic 5xHRE (Promega; E1751)	(Hammond et al., 2006)
pHRE-LUC	pGL3-basic 5xHRE (Promega; E1751)	(Hammond et al., 2006)
SpCas9-GFP-RRM2B_1/3	pSpCas9(BB)-2A-GFP (Addgene; 48138)	This paper
SpCas9-GFP-RRM2B_2	pSpCas9(BB)-2A-GFP (Addgene; 48138)	This paper